Rapid Laser Nanomanufacturing and Direct Patterning of 2D Materials on Flexible Substrates – 2DFlex

Zabihollah Ahmadi¹, Parvin Fathi-Hafshejani¹, Emre Kayali², Majid Beidaghi², Masoud Mahjouri-Samani^{1*}

¹ Electrical and Computer Engineering Department, Auburn University, Auburn, AL, USA 36849

² Department of Mechanical and Material Engineering, Auburn University, Auburn, AL, USA 36849

*Address correspondence to mahjouri@auburn.edu

Abstract

Direct synthesis, large-scale integration, and patterning of two-dimensional (2D) quantum materials (e.g., MoS₂, WSe₂) on flexible and transparent substrates are of high interest for the flexible and conformal device applications. However, the growth temperature (e.g., 850 °C) of the emerging 2D materials in the common gas-phase synthesis methods are well beyond the tolerances limit of flexible substrates, such as polydimethylsiloxane (PDMS). In addition, random nucleation and growth process in most growth systems limits the predicted integration and patterning freedoms. Here, we report a rapid direct laser crystallization and mask-free large-scale patterning of MoS₂ and WSe₂ crystals on PDMS substrates. A thin layer of stoichiometric amorphous 2D film is first laser-deposited via pulsed laser deposition (PLD) system onto the flexible substrates followed by a controlled crystallization and direct writing process using a tunable nanosecond laser (1064 nm). The influences of pulse duration, number of pulses, and the thickness of the deposited amorphous 2D layer on the crystallization of 2D materials are discussed. Optical spectroscopy and electrical characterizations are performed to confirm the quality of crystallized 2D materials on flexible substrates. This novel method opens up a new opportunity for the crystallization of complex patterns directly from computer-aided design models for the future 2D materials-based wearable, transparent, and flexible devices.

Keywords: 2D materials, flexible electronics, additive nanomanufacturing, laser processing

Introduction

Compared to conventional rigid devices, stretchable and flexible devices can be attached to irregular and deformed surfaces. Such devices are gradually used in emerging new areas such as wearable devices, soft robotics, electronics skin, and flexible display.^[1] New biomedicine and healthcare applications of flexible and stretchable devices have been emerged due to intrinsic mechanical properties, excellent compliance, biocompatibility, and conformability to tissue surfaces.^[2] Also, flexible photonics is now enabling a wide range of emerging applications including board-level optical interconnects,^[3-6] optomechanical tuning,^[7-9] epidermal monitoring, ^[10] strain sensing,^[11] and conformal photonics.^[12, 13]

Over the past few years, 2D quantum materials have been considered as promising candidates for future flexible and transparent device applications due to their outstanding mechanical, electrical, and optical properties. [14-21] In addition, these atomically-thin sheets afford the ultimate thickness scalability desired in a variety of essential material categories including semiconductors, insulators, conductors, and superconductors. [22-24] The majority of 2D-based electronic devices use chemically or mechanically exfoliated 2D sheets.^[25] At present, only relatively small samples of these 2D materials can be generated with mechanical exfoliation. On the other hand, poor layer thickness and size uniformity, uncontrolled nanosheet orientations, and contamination between layers are some examples that prevent the viability of chemical exfoliation in real applications. [26-^{28]} Chemical vapor deposition (CVD) is a common approach for generating high-quality, largearea 2D thin films. [29-32] However, due to high growth temperatures (approximately 700–900 °C) required for the decomposition of transition metal dichalcogenides (TMDs) precursor gases, CVD and other gas-phase synthesis techniques are not suitable for stretchable and flexible substrates. Most recently, magnetron sputtering of TMD targets has been demonstrated to directly deposit large-area amorphous MoS₂ film at low temperatures (250 °C). Researchers used a broadband pulsed flash lamp (200-1500nm) and laser annealing (continuous wave 532, 660, 785, and 830 nm lasers) processes to successfully crystallize the sputtered amorphous layers on flexible substrates. [17, 33] Although these methods showed the crystallization of 2D materials, complex patterning and large-scale integration are not yet reported to date. As 2D devices become more complex (e.g., numerous 2D materials, layers, shapes, etc.), the patterning steps (lithographically and subsequently etching unwanted areas of 2D material) can become expensive, time-consuming, and sometimes incompatible with flexible substrates.^[34] Material printing and additive manufacturing have emerged as new fabrication concepts that allow for the transfer of liquid-based 2D inks onto flexible substrates for device printing. [35, 36] For instance, inkjet printing based on commercial jet printing devices is widely used because of its direct-writing, low-temperature, mask-free, and its compatibility with flexible substrates.^[35] However, the ink is made via chemical exfoliation and slurry formation techniques that suffer from contamination, nonuniformity, and precise thickness control issues. Moreover, the nozzles used in inkjet printing can be clogged frequently. To the best of our knowledge, the ability to directly synthesize crystalline TMDs with patterning complex shapes on flexible substrates has remained elusive.

Here, we report an approach to directly crystallize and integrate complex patterns of 2D materials (MoS₂, WSe₂) onto the flexible substrates enabling the future conformal and transparent optoelectronic and photonic devices. Controlled crystallization and direct writing processes are achieved by a precise laser processing of stoichiometric amorphous 2D films on flexible substrates. Selective and localized photothermal heating induced by a nanosecond laser coupled into a computer-controlled laser scanner system is used to rapidly pattern complex shapes and transform

2D materials from an amorphous phase to a polycrystalline phase. The influence of laser pulse duration, the number of pulses, and thickness of the as-deposited amorphous 2D layer on the crystallization of 2D materials are investigated. This laser crystallization method opens up new routes for the synthesis and the mask-less patterning of intricate patterns of 2D materials onto flexible substrates.

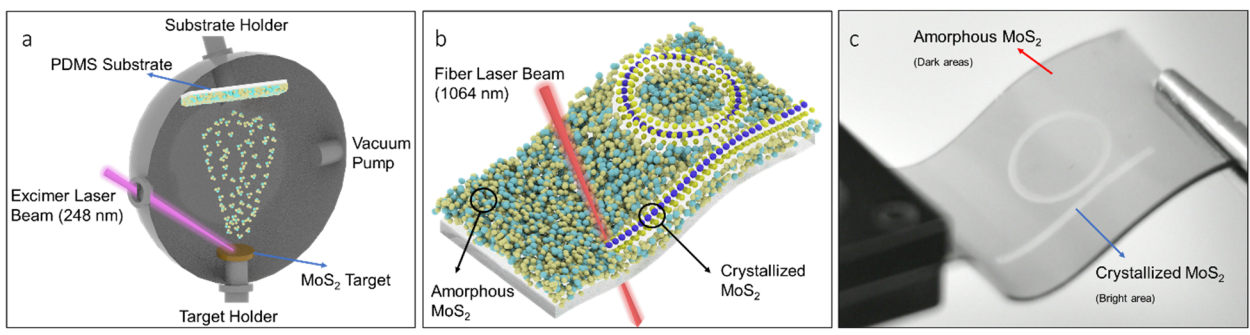


Figure 1. Schematic diagrams of the two-step deposition and crystallization techniques. A pulsed laser deposition system is used to deposit a thin layer of a stoichiometric amorphous 2D layer onto PDMS substrates (a), followed by direct laser crystallization and patterning of this amorphous 2D layers (b). An optical image of a crystallized MoS₂ pattern (bright lines) on a PDMS substrate (c).

Results and discussion

Figure 1 shows the schematics representation of the laser deposition, crystallization, and patterning processes used for the direct integration of 2D materials onto flexible PDMS substrates. In this approach, a pulsed laser deposition (PLD) system (figure 1(a)) was used to deposit thin films of stoichiometric amorphous MoS2 and WSe2 materials onto the PDMS substrates. 1-inch diameter pellets of hardly pressed MoS₂ and WSe₂ powders were used as ablation targets. An excimer laser (COMPexPro, KrF) with λ=248 nm was used for target ablation at a 40° angle of incidence and 5 Hz repetition rate. Targets (MoS₂ and WSe₂) were placed separately on a target carousel inside a spherical chamber (21 inches in diameter). The resultant laser spot size and fluence on the MoS₂ and WSe₂ targets were 2 × 5 mm and 1.5 J cm⁻², respectively. The pressure inside the ablation chamber was lowered to \sim 5 × 10⁻⁶ Torr for deposition, and the substrate-target distance was set at 7 cm. While keeping the aforementioned PLD parameters constant throughout the experiments, a series of samples (MoS₂, WSe₂) with different thicknesses were prepared by controlling the number of laser pulses (see supporting information figure S1). As-deposited amorphous thin films on PDMS substrates were placed inside a costume-designed environmental processing chamber for subsequent laser crystallization (figure 1(b)) and pattering processes under the argon gas environment at atmospheric pressure and room temperature. To avoid surface oxidation during the crystallization process, the chamber was first flushed by argon gas for a few minutes, and then the argon gas flow rate was kept constant at 200 sccm during the whole experiment. For crystallization and patterning, the laser beam from a nanosecond pulsed fiber laser with $\lambda = 1064$ nm (0 to 130 W), tunable nanosecond pulses, 5–2000 ns in 63 waveforms, with pulse energy from ranging 0.04 to 1.57 mJ and a repetition rate 100 KHz) was coupled to a galvo scanner with a 13 µm focal point. The process parameters (e.g., power, pulse duration, number of pulses, etc.) for each specific pattern were controlled by a laser marking software (Laser Studio Professional).

The low thermal conductivity of the amorphous 2D materials and the PDMS substrate results in a poor heat transfer, which can severely damage and deform the substrate if the crystallization process is not spatiotemporally controlled. Therefore, it is essential to utilize a crystallizing process that can overcome this limitation. Time-resolved infrared laser crystallization method allowed us to controllably couple a precise amount of energy and hence heat the amorphous 2D layer for selective phase transformation. In this controlled laser-material interaction process, the heat penetration depth was controlled in a way that there is enough time for thermal energy to crystallize the amorphous 2D material without damaging the underlying PDMS substrate. The tunable nanosecond fiber laser (1064 nm) was used for laser processing since the PDMS has extremely low optical absorption in 1064 nm wavelength^[37]. Comprehensive experiments were performed to find the influence of laser pulse-width (ranging from 10 ns to 620 ns), the number of laser pulses per spot (ranging from 1 to 40), and the thickness of the as-deposited amorphous layer on the crystallization of 2D materials (see supporting information **figure S2**). These allowed us to identify the best processing conditions for further crystallization and patterning of complex shapes.

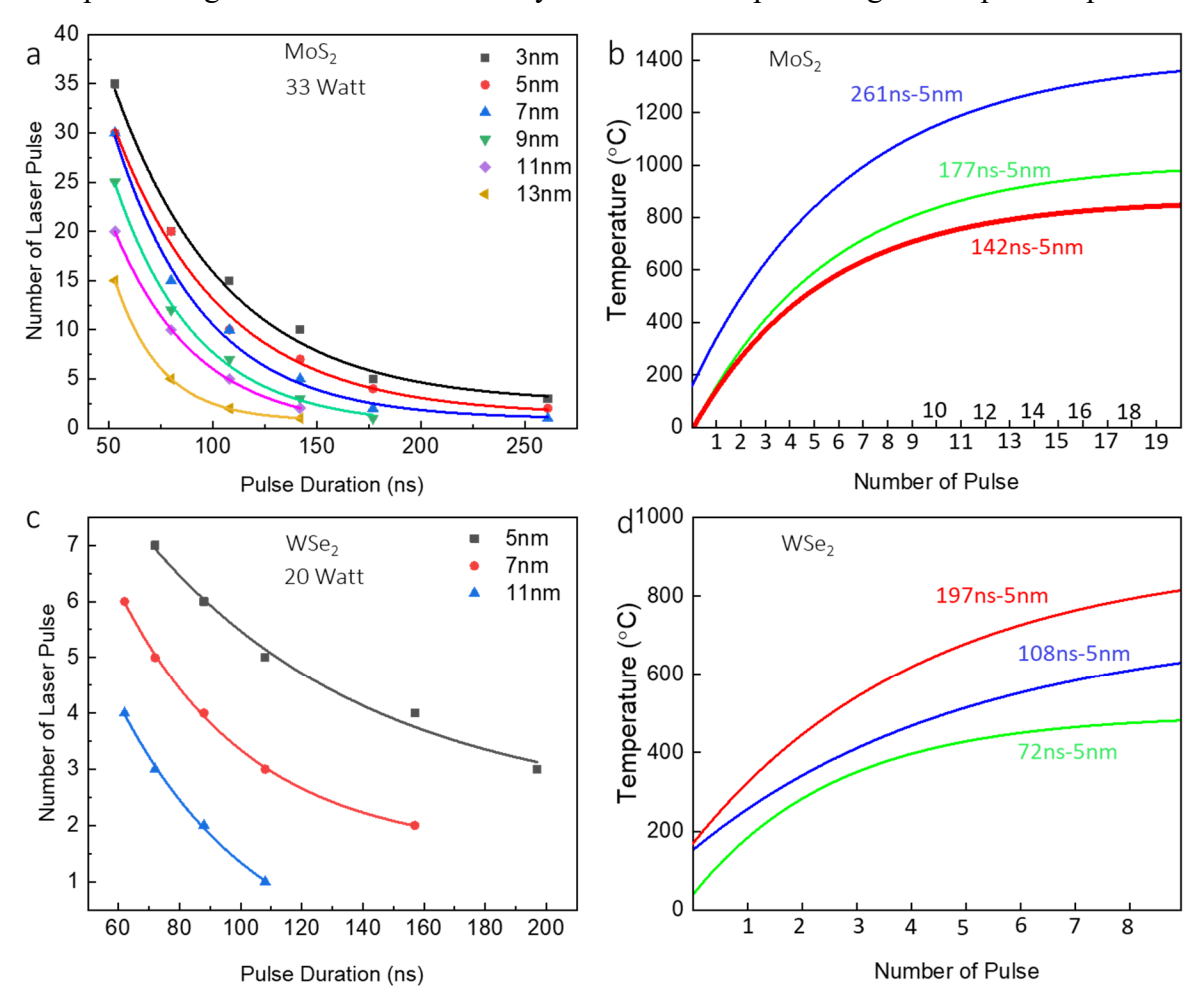


Figure 2. The effect of laser irradiation on amorphous 2D MoS₂ (a) and WSe₂ (c) films. Each graph represents the effect of laser pulse-width and the number of pulses on the crystallization of amorphous layers with various thicknesses. The lines indicate the locations where good crystals can be formed for each thickness, depending on the laser pulse duration and number of pulses. The graphs in (b) and (d) show the COMSOL simulation results for the average heat generated by the interaction of a 1064nm laser beam at the indicated pulse durations with 5nm-thick amorphous layers of MoS₂ and WSe₂, respectively.

The symbols in each panel of figure 2(a), (c) indicate the processing parameters locations where good 2D MoS₂ and WSe₂ crystals were obtained, respectively. The curves are fitted to provide processing guidance. Employing the process parameters on the curves for each pulse-width resulted in the formation of high-quality 2D crystals without creating any damage to the PDMS substrate. However, the laser parameters to the right and above of the curves in figure 2a resulted in the burning of PDMS or the evaporation of the amorphous 2D materials. On the other hand, employing process parameters to the left and below the curves resulted in the formation of lowquality 2D crystals or did not affect the amorphous layer (see Supporting Information, figure S3). As it is shown in figure 2(a) and (c), we observed that exposing the amorphous films to longer laser pulse-widths required less number of the laser pulses for crystallization and vice versa. Also, increasing the thickness of the as-deposited amorphous layers of 2D MoS₂ and 2D WSe₂ required shorter laser pulse-widths and less number of pulses to crystallize the amorphous layers, as shown in figure 2(a) and (c). The increase in the thickness of amorphous MoS₂ and WSe₂ films results in stronger absorption of 1064nm laser beam and hence higher local heat. In addition, the widths of the crystalline lines were smaller when crystalized by shorter pulse durations. This could be attributed to heat formation and dissipation time. When the laser pulse-width is small (e.g., 70 ns), the generated heat has less time to dissipate in the amorphous materials, hence inducing a smaller heat-affected zone. In contrast, a higher laser pulse-width (e.g., 261ns) provides a longer time for heat formation and dissipation to an area outside the laser spot, causing a larger heat-affected zone and hence a larger crystalline line width. Also, it should be noted that the energy per pulse is higher for longer pulse-width than the shorter ones, defined by the laser operating mechanism. According to experimental observations, the laser pulse-widths beyond 261ns always resulted in the evaporating or damaging of the amorphous materials and the PDMS substrate (see supporting information, figure S4). Parameters that results in evaporation of the materials may be used for subtractive nanomanufacturing of the unwanted 2D materials from the substrate (i.e., removal of remaining amorphous lasers).

Modeling of nanosecond pulsed laser interactions with both MoS₂ and WSe₂ materials was investigated using the COMSOL Multiphysics software package. The average heat generated by a nanosecond laser interaction with amorphous 2D materials versus the number of pulses is shown in **figure 2(b)**, **(d)** (see supporting information for detail, **figure S5**). Thermal properties of amorphous MoS₂ and WSe₂ were used from previous works [38],[41]. For example, irradiation of a 5nm amorphous MoS₂ layer on PDMS substrate using a laser with 261ns pulse-width and 2 and 3 pulses results in a localized heat around ~600 and 700°C, respectively. In addition, irradiations beyond 4 laser pulses would raise the localized heat above 700°C that decomposes and evaporates the 2D materials from the PDMS substrates. These results indicated the importance of a time-resolved nonequilibrium laser processing approach to provide a sufficient temperature in a short time to crystallize the as-deposited amorphous layer on flexible platforms without damaging the underlying substrates.

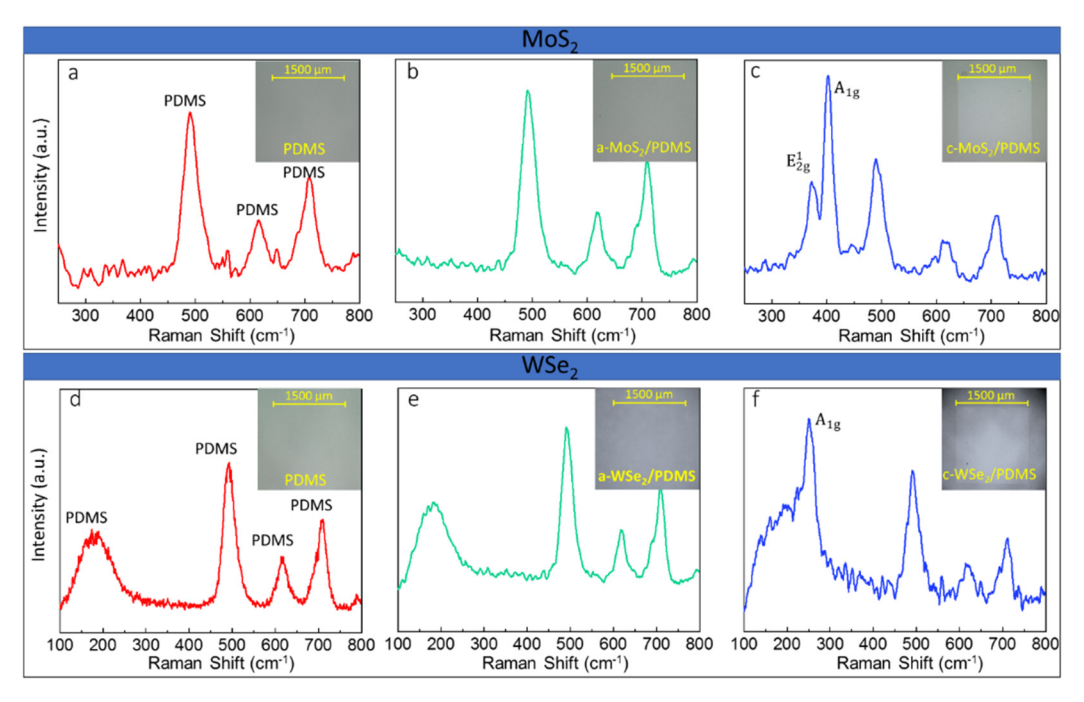


Figure 3. Optical images and Raman spectra of the samples before and after the laser deposition and crystallization processes. Optical images and Raman spectra of bare PDMS substrates (**a**, **d**), amorphous MoS₂ and WSe₂ films on PDMS substrates (**b**, **e**), and ~7nm MoS₂ and WSe₂ layer on PDMS substrates crystallized by 12 pulses (108 ns pulse duration, 33W) and 3 pulses (108 ns pulse duration, 20W), respectively(**c**, **f**). Both the bare PDMS and amorphous 2D materials on the PDMS substrates show similar Raman peaks since the amorphous layer does not have any Raman fingerprints. The laser-crystallized materials, however, show very sharp Raman signatures at 375 and 405 cm⁻¹, corresponding to crystalline MoS₂, and at 250 cm⁻¹, corresponding to crystalline WSe₂ materials.

Raman spectroscopy was used to monitor the crystallization evolution and quality of the laser processed amorphous materials on the PDMS substrates. The Raman spectra were obtained at room temperature using a 532nm excitation laser from bare PDMS substrates (figure 3(a), (d)), amorphous MoS₂ and WSe₂ layer coated onto the PDMS substrates (figure 3(b), (e), and laser crystallized MoS₂ (c-MoS₂) and WSe₂ layers on the PDMS substrates (figure 3(c), (f)). The Raman spectra of PDMS and amorphous layers on the PDMS are similar since amorphous MoS₂ and WSe₂ films do not have any specific Raman signatures. However, the active Raman modes of MoS₂ crystals at ~ 372 cm⁻¹ (E¹_{2g}) and ~ 402 cm⁻¹ (A¹_g), and WSe₂ crystal at ~ 250 cm⁻¹ (A¹_g) are clearly observed in figure 3(c), (f) after the laser crystallization process. The inset in each image shows the corresponding optical images of the pure PDMS, PDMS with amorphous 2D layer, and PDMS with the crystallized 2D layer. As shown by the inset images of figure 3, the crystallized materials became optically brighter than the non-crystallized materials, possibly due to the index change. As reported by others. [39] the phonon confinement model can be used to determine the estimated sizes of the grains that are proportional to the inverse of Raman peak FWHM. For instance, the FWHM of A_g^1 modes in MoS₂ and WSe₂ show ~ 15 cm⁻¹ and 25 cm⁻¹, indicating grain sizes, approximately tens of nm. The peak frequencies and shapes of the MoS₂ and WSe₂ Raman spectra are comparable to crystallized MoS₂ and WSe₂ by laser crystallization techniques, reported by others ^[17, 40]. Also, compared to the single-crystalline 2D materials grown by, for example, CVD method, [41] the Raman peaks show similar behavior with slightly broader widths due to the nanoscale crystalline domain sizes formed in this process. Accordingly, our approach is not only comparable with other methods in terms of crystalline quality but also has the ability to create complex patterns.

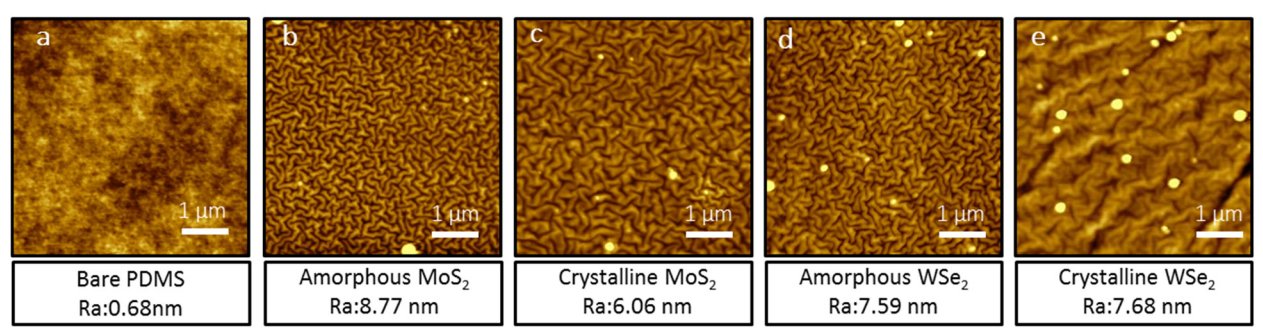


Figure 4. AFM image and roughness (Ra) of a bare PDMS (a), as-deposited amorphous MoS₂ on PDMS (b), MoS₂ crystallized by 8 pulses (108ns pulse duration, 33W) on PDMS (c), as-deposited amorphous WSe₂ on PDMS (d), and WSe₂ on PDMS crystallized by 3 pulses (108 ns pulse duration, 20W) (e). After PLD of amorphous materials on PDMS, small wrinkles were observed (b, d), and after the laser crystallization, the wrinkle sizes became larger (c, e).

Figure 4a-e shows the AFM topography of the bare PDMS as well as amorphous and crystalline MoS₂ and WSe₂ films on the PDMS substrates. The surface roughness of the bare PDMS substrate was about 0.68 nm. During the deposition of the amorphous 2D materials, PLD increased the roughness to 8.77 nm and 7.59 nm for MoS₂ and WSe₂, respectively. After the laser crystallization, the roughness was 6.06 nm and 7.68 nm for MoS₂ and WSe₂, respectively. Surface wrinkles are created possibly due to the high vacuum deposition as well as laser-produced plasma during the PLD process. [42] The wrinkles observed in the crystallized MoS2 and WSe2 fabricated by our method are similar to the works reported in this area. [17] The ability to directly integrate 2D and other quantum materials with desired patterns and shapes onto the flexible substrates is highly demanded for applications ranging from electronics to photonics and energy to sensing devices. Utilizing our approach, we demonstrated the formation of various 2D material-based patterns on the PDMS substrate. For instance, figure 5(a), (b) demonstrates the fabricated crystalline ~5nm WSe₂-based photonics Mach Zehnder interferometer and electronic circuit patterns, respectively. The laser power, pulse duration, and number of pulses used for crystallization of patterns in figure 5(a), (b) are 20W, 157ns and 4, respectively. Our crystallization and pattering process allows the realization of complex and arbitrary and pre-defined patterns on flexible substrates.

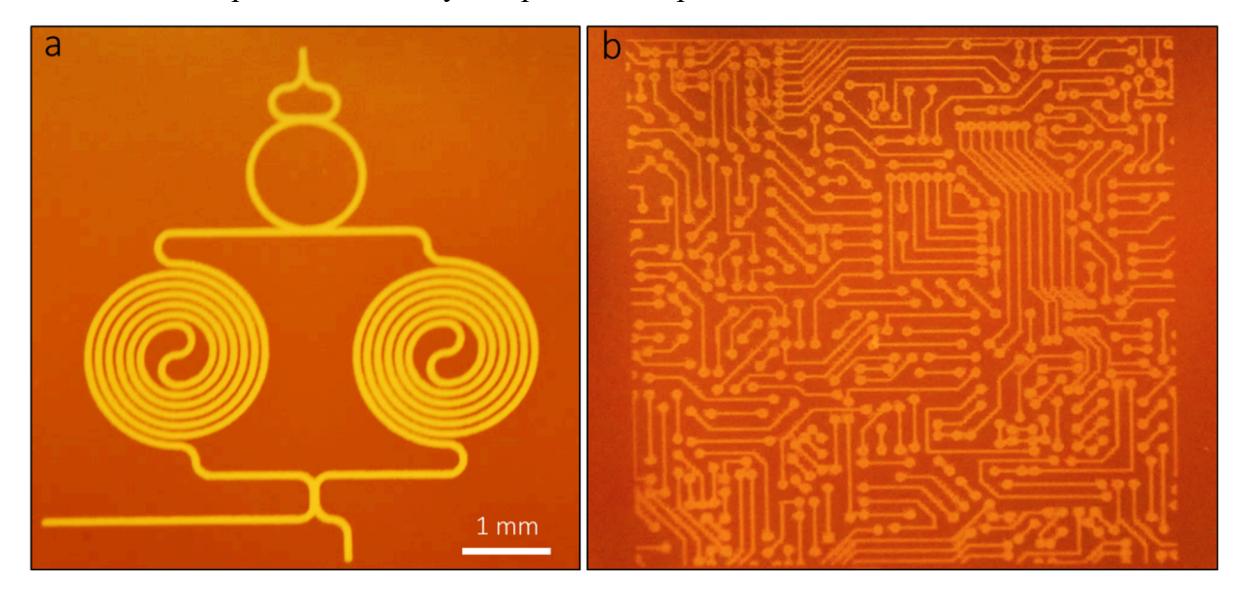


Figure 5. Examples of patterned 2D crystals on the PDMS substrates. A photonics Mach Zehnder interferometer (a), an electronics circuit board (b). The scale bar is the same for both images.

To achieve an insight into the flexibility of the fabricated device, the IV characteristic and resistance of the crystallized MoS₂ sample were measured by depositing gold contact electrodes. To fabricate such devices, we first crystallized a large area of amorphous MoS₂ on PDMS (power: 33W, pulse duration: 108ns, and the number of pulses: 10) followed by the deposition of gold contacts through photolithography and sputtering processes. Figure 6(a) shows the photograph of the fabricated devices on the PDMS substrate. Figure 6(b) shows a three-dimensional illustration of the crystalline 2D materials with two gold contacts (inset image is the optical image of the fabricated device). Figure 6(c) shows the IV characteristics of a 5 nm c-MoS₂ device. The resistance increased gradually in inverse proportion to the bending radius (figure 6(d)). Different colors in figure 6(d) show the variations in different measurement runs. Bending the film (r=4 mm
bending radius
r = 20 mm) led to an increase in R compared to the flat condition (8G Ω) due to the mechanical deformation of 2D c-MoS₂. A considerable decrease in electrical conductivity can arise since defects and cracks can be introduced into the MoS₂ nanocrystalline structures. In cases where the remaining amorphous portion of the film may cause an issue in the device performance, the exact knowledge gained in this paper was utilized to selectively remove the unwanted amorphous layers from the substrates. First, the optimum crystallization process parameters were first used to crystallize the desired patterns, and then vaporization process parameters (e.g., 26W, 157ns, 15LP) were used to selectively evaporate the unwanted amorphous portion of deposition without any damage to the PDMS substrates. (See figure S6 in the supporting information).

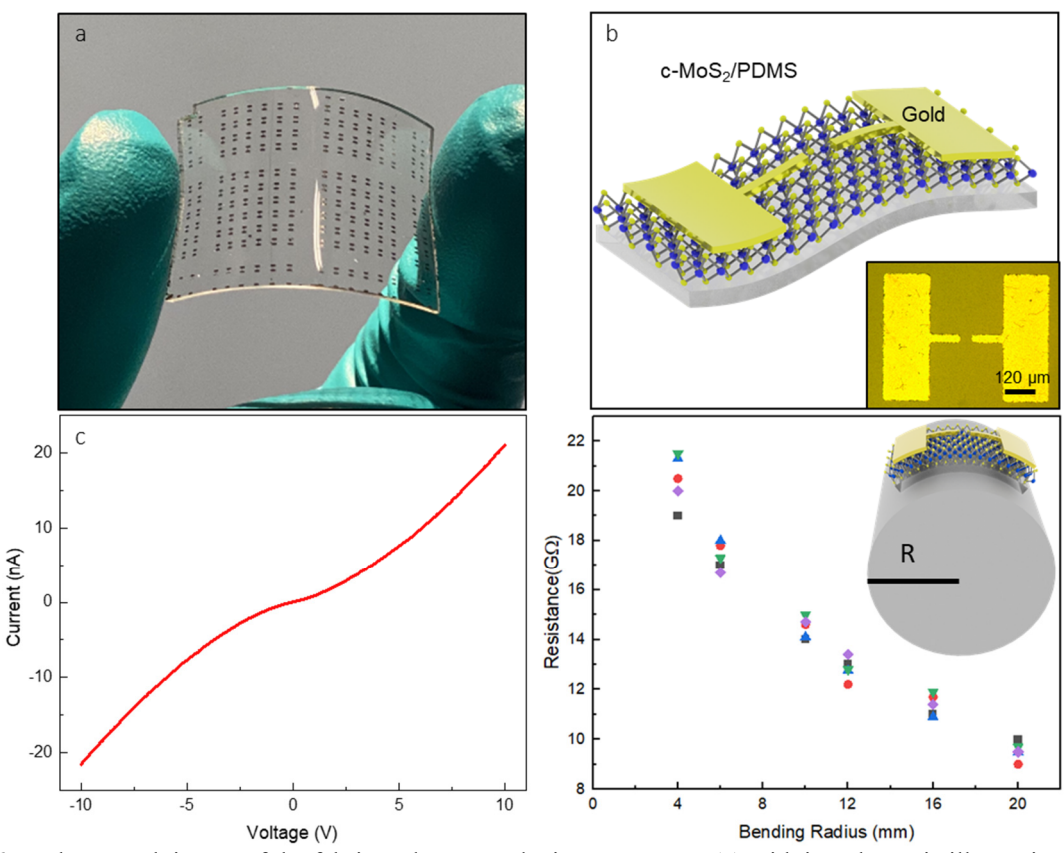


Figure 6. A photograph image of the fabricated c-MoS₂ devices on PDMS (a) with its schematic illustration (b). The onset in b is the optical image of a single device. An example of the IV characteristics from a 5nm thick crystallized MoS₂ device on PDMS (c), resistance of a fabricated device according to the bending radius under tensile strain (d).

Conclusion

In summary, we presented a direct laser crystallization and large-area complex patterning of PLD deposited amorphous 2D materials (MoS₂, WSe₂) on flexible PDMS substrates. We demonstrated that a tunable nanosecond (1064 nm) laser has allowed us to controllably couple a precise amount of energy and hence heat to the amorphous 2D layer for selective phase transformation. In this controlled time-resolved laser-material interaction process, the localized and selective crystallization was controlled by optimizing the pulse duration and the number of the laser pulse in each spot in a way that there is enough time for photothermal energy to crystallize the amorphous 2D material without damaging the underlying PDMS substrate. COMSOL Multiphysics simulation package was used to model the heat formation caused by the interaction of a nanosecond pulse laser with 2D a-MoS₂ and a-WSe₂ materials. Furthermore, we showed the capability of this laser crystallization process to make any complex shapes and patterns. This novel method opens up a new opportunity for the future 2D materials-based wearable, transparent, and flexible optoelectronic, photonic, and sensing devices.

Supporting Information Available

Supporting Information is available online.

Acknowledgments

This material is based upon work partially supported by the U.S. National Science Foundation (NSF) under grant No. 1923363, and Auburn University Intermural Grant Program (IGP-VPR 180247). We thank Alabama Micro/Nanoelectronic Science and Technology Center (AMNSTC) for providing access to the cleanroom facility.

Author Contributions

Z.A. designed and performed laser synthesis and processing experiments, materials characterization, and data analysis. P.F. participated in the laser processing experiment. E.K. and M. B. participated in AFM measurements, characterization, and manuscript preparation. M.M.S. led the project, participated in experimental design, data acquisition and analysis, discussions, and manuscript preparation. All of the authors commented on the manuscript.

Conflict of Interest

The authors declare no conflict of interest.

References

- 1. Mohandas, N., et al., *Deciphering the role of epigenetics in self-limited epilepsy with centrotemporal spikes*. Epilepsy Res, 2019. **156**: p. 106163.
- 2. Bao, Z.N. and X.D. Chen, *Flexible and Stretchable Devices*. Advanced Materials, 2016. **28**(22): p. 4177-4179.
- 3. Bosman, E., et al., *Highly Reliable Flexible Active Optical Links*. Ieee Photonics Technology Letters, 2010. **22**(5): p. 287-289.

- 4. Choi, C.C., et al., Flexible optical waveguide film fabrications and optoelectronic devices integration for fully embedded board-level optical interconnects. Journal of Lightwave Technology, 2004. **22**(9): p. 2168-2176.
- 5. Dangel, R., et al., *Development of Versatile Polymer Waveguide Flex Technology for Use in Optical Interconnects*. Journal of Lightwave Technology, 2013. **31**(24): p. 3915-3926.
- 6. Li, L., et al., A Fully-Integrated Flexible Photonic Platform for Chip-to-Chip Optical Interconnects. Journal of Lightwave Technology, 2013. **31**(24): p. 4080-4086.
- 7. Zhu, L., et al., *Flexible photonic metastructures for tunable coloration*. Optica, 2015. **2**(3): p. 255-258.
- 8. Zou, Y., et al., Solution Processing and Resist-Free Nanoimprint Fabrication of Thin Film Chalcogenide Glass Devices: Inorganic-Organic Hybrid Photonic Integration. Advanced Optical Materials, 2014. **2**(8): p. 759-764.
- 9. Chen, Y., H. Li, and M. Li, *Flexible and tunable silicon photonic circuits on plastic substrates*. Scientific Reports, 2012. **2**(1): p. 622.
- 10. Gao, L., et al., *Epidermal photonic devices for quantitative imaging of temperature and thermal transport characteristics of the skin.* Nature Communications, 2014. **5**(1): p. 4938.
- 11. Fan, L., et al., *Direct fabrication of silicon photonic devices on a flexible platform and its application for strain sensing.* Optics Express, 2012. **20**(18): p. 20564-20575.
- 12. Kamali, S.M., et al., *Decoupling optical function and geometrical form using conformal flexible dielectric metasurfaces.* Nature Communications, 2016. **7**(1): p. 11618.
- 13. Zhou, W. and Z. Ma, *Breakthroughs in Photonics 2012: Breakthroughs in Nanomembranes and Nanomembrane Lasers.* IEEE Photonics Journal, 2013. **5**(2): p. 0700707-0700707.
- 14. Cain, J.D., et al., *Emerging opportunities in the two-dimensional chalcogenide systems and architecture.* Current Opinion in Solid State & Materials Science, 2016. **20**(6): p. 374-387.
- 15. Novoselov, K.S., et al., *Electric field effect in atomically thin carbon films*. Science, 2004. **306**(5696): p. 666-669.
- 16. Bolotsky, A., et al., *Two-Dimensional Materials in Biosensing and Healthcare: From In Vitro Diagnostics to Optogenetics and Beyond.* Acs Nano, 2019. **13**(9): p. 9781-9810.
- 17. Kim, R.H., et al., *Photonic crystallization of two-dimensional MoS2 for stretchable photodetectors.* Nanoscale, 2019. **11**(28): p. 13260-13268.
- 18. Sirota, B., N. Glavin, and A.A. Voevodin, *Room temperature magnetron sputtering and laser annealing of ultrathin MoS2 for flexible transistors.* Vacuum, 2019. **160**: p. 133-138.
- 19. Akinwande, D., N. Petrone, and J. Hone, *Two-dimensional flexible nanoelectronics*. Nature Communications, 2014. **5**(1): p. 5678.
- 20. Muratore, C., A.A. Voevodin, and N.R. Glavin, *Physical vapor deposition of 2D Van der Waals materials: a review.* Thin Solid Films, 2019. **688**: p. 137500.
- 21. Elafandi, S., et al., Gas-Phase Formation of Highly Luminescent 2D GaSe Nanoparticle Ensembles in a Nonequilibrium Laser Ablation Process. Nanomaterials (Basel, Switzerland), 2020. 10(5): p. 908.
- 22. Fang, H., et al., *High-Performance Single Layered WSe2 p-FETs with Chemically Doped Contacts*. Nano Letters, 2012. **12**(7): p. 3788-3792.
- 23. Lee, G.H., et al., Flexible and Transparent MoS2 Field-Effect Transistors on Hexagonal Boron Nitride-Graphene Heterostructures. Acs Nano, 2013. 7(9): p. 7931-7936.
- 24. Meric, I., et al., *Graphene Field-Effect Transistors Based on Boron-Nitride Dielectrics*. Proceedings of the Ieee, 2013. **101**(7): p. 1609-1619.

- 25. Cao, W., J. Wang, and M. Ma, *Exfoliation of Two-Dimensional Materials: The Role of Entropy*. Journal of Physical Chemistry Letters, 2019. **10**(5): p. 981-986.
- 26. Coleman, J.N., et al., *Two-Dimensional Nanosheets Produced by Liquid Exfoliation of Layered Materials*. Science, 2011. **331**(6017): p. 568-571.
- 27. Niu, L.Y., et al., Salt-Assisted High-Throughput Synthesis of Single- and Few-Layer Transition Metal Dichalcogenides and Their Application in Organic Solar Cells. Small, 2014. **10**(22): p. 4651-4657.
- 28. Smith, R.J., et al., *Large-Scale Exfoliation of Inorganic Layered Compounds in Aqueous Surfactant Solutions*. Advanced Materials, 2011. **23**(34): p. 3944-+.
- 29. Yu, J.X., et al., Synthesis of high quality two-dimensional materials via chemical vapor deposition. Chemical Science, 2015. **6**(12): p. 6705-6716.
- 30. Zhou, J.D., et al., *A library of atomically thin metal chalcogenides*. Nature, 2018. **556**(7701): p. 355-+.
- 31. Azam, N., et al., Accelerated synthesis of atomically-thin 2D quantum materials by a novel laser-assisted synthesis technique. 2D Materials, 2019. 7(1): p. 015014.
- 32. Ahmadi, Z., et al., *Application of lasers in the synthesis and processing of two-dimensional quantum materials.* Journal of Laser Applications, 2019. **31**(3): p. 031202.
- 33. McConney, M.E., et al., *Direct synthesis of ultra-thin large area transition metal dichalcogenides and their heterostructures on stretchable polymer surfaces (vol 31, pg 967, 2016)*. Journal of Materials Research, 2016. **31**(7): p. 975-975.
- 34. Song, I., et al., *Patternable Large-Scale Molybdenium Disulfide Atomic Layers Grown by Gold-Assisted Chemical Vapor Deposition*. Angewandte Chemie International Edition, 2014. **53**(5): p. 1266-1269.
- 35. Huang, L., et al., *Graphene-based conducting inks for direct inkjet printing of flexible conductive patterns and their applications in electric circuits and chemical sensors.* Nano Research, 2011. **4**(7): p. 675-684.
- 36. Hossain, R.F., et al., *Biocompatible, large-format, inkjet printed heterostructure MoS2-graphene photodetectors on conformable substrates.* npj 2D Materials and Applications, 2017. **1**(1): p. 28.
- 37. Ahmadi, Z., et al., Self-limiting laser crystallization and direct writing of 2D materials. International Journal of Extreme Manufacturing, 2019. **1**(1): p. 015001.
- 38. Chiritescu, C., et al., *Ultralow Thermal Conductivity in Disordered, Layered WSe<sub>2</sub> Crystals.* Science, 2007. **315**(5810): p. 351.
- 39. Spanier, J.E., et al., Size-dependent properties of \${\mathrm{CeO}}_{2\ensuremath{-}}y}\$ nanoparticles as studied by Raman scattering. Physical Review B, 2001. **64**(24): p. 245407.
- 40. Rai, R.H., et al., *Pulsed laser annealing of amorphous two-dimensional transition metal dichalcogenides.* Journal of Vacuum Science & Technology A, 2020. **38**(5): p. 052201.
- 41. Yang, L., et al., Lattice strain effects on the optical properties of MoS2 nanosheets. Scientific Reports, 2014. **4**(1): p. 5649.
- 42. Park, H.-G., et al., Control of the wrinkle structure on surface-reformed poly(dimethylsiloxane) via ion-beam bombardment. Scientific Reports, 2015. **5**(1): p. 12356.